The dual-frequency zero-backward scattering realized in a hybrid metallo-dielectric nanoantenna

The dual-frequency zero-backward scattering realized in a hybrid metallo-dielectric nanoantenna

Chaowei Xu, Kaiyang Cheng, Quan Li, Xiaobing Shang, Chao Wu (iD), Zeyong Wei, Xiaoming Zhang, and Hongqiang Li

View Online   **Export Citation**   **CrossMark**

ARTICLES YOU MAY BE INTERESTED IN

The dual-frequency zero-backward scattering realized in a hybrid metallo-dielectric nanoantenna

View Online   Export Citation   CrossMark

Chaowei Xu,[1,2] Kaiyang Cheng,[1,2] Quan Li,[1,2] Xiaobing Shang,[2] Chao Wu,[1,2] (iD) Zeyong Wei,[1,2] Xiaoming Zhang,[3,a] and Hongqiang Li[1,2,a]

AFFILIATIONS

[1] School of Physical Science and Engineering, Tongji University, Shanghai 200092, China
[2] Institute of Dongguan-Tongji University, Dongguan 523808, China
[3] College of Physics Science and Engineering Technology, Yichun University, Yichun, Jiangxi Province 336000, China

[a] Corresponding author E-mail address: zhangxm@idtu.cn, hqlee@tongji.edu.cn

ABSTRACT

In this paper, we propose a hybrid metallo-dielectric core-shell nanorod for the Kerker-type effect at two different frequencies. The effect arises from the interference of the scattering waves of the nanorod, which are generated by the magnetic dipole moment (MD) of the high-index hollow particle and the electric dipole moment (ED) induced in both metallic and dielectric particles. Interestingly, we find that such kind of unidirectional radiation properties, (i.e., zero back scattering occurring at dual frequencies) can be sustained with a single nanorod, which usually being equivalent to a local electric dipole source. The effect of substrate is also considered to investigate the typical experimental realization for the dual-frequency unidirectionalities of the nanoantenna. Furthermore, the unidirectionality can be further improved by the design of one-dimensional array of the hybrid nanoantenna. Our results could provide an additional degree of freedom for light scattering manipulation, and widen the versatile applications in nanoantennas, optical sensor, light emitters, as well as photovoltaic devices.

I. INTRODUCTION

Light scattering, as a primary physics process in light-matter interactions, have always been a focus of researchers for a long time, and have widely been applied in optical communication, astrophysics, chemistry, biophysics and material science, etc.[1–3] In recent years, with the development and prevalence of nanoscale fabrication, the size, shape and material of subwavelength-sized nanostructures can be finely tuned with respective to the need of utility, such that the control of light scattering in subwavelength scale have been obtained more and more attention. A lot of nanophotonic applications, such as nanoantennas, and nanoplasmonic sensor, etc., have been proposed.[4–7] Dielectric response of subwavelength-sized nanostructures, in presence of electric dipole (ED) moments and magnetic dipole (MD) moments,[8,9] can give rise to exotic effects, such as superscatter,[10] invisibility cloak,[11] and directionality, etc.[12,13]

It is well known that unidirectional scattering has great application potential in nanoantenna,[14,15] bio-sensing,[16,17] light emission[18] and photovoltaic device.[19] The ED and MD of an appropriately designed nanoantenna, under certain excitation, could be overlapped with equal amplitudes at certain frequencies, as known as first Kerker condition.[20,21] And the directionality with zero-backscattered field can be achieved by suppressing backward scattering relative to the direction of the incoming wave. By embedding a gold nanoring in a homogenous host medium, ED and electric quadrupole moments also cancel with each other.[8] Due to the lack of natural magnetism at optical frequencies, the artificial magnetic responses of metal antennas coupled with incident light are explored. A gold U-shaped split-ring resonator can also support the electric dipole, quadrupole, and magnetic dipole moments to realize a compact directional optical antenna.[22–24] A metallic trimer antenna can support a highly spectrally tunable magnetic

dipole mode with its amplitude comparable to that of an electric dipole mode, which satisfy the Kerker conditions.[25,26] However, the ohmic losses and saturation effects of metallic materials limit the performance and application of metal structures in optical waveband.

Recent studies indicate that strong magnetic resonance can be excited in high dielectric materials without ohmic loss in the near-infrared and visible regions.[27–34] GaAs pillars are experimentally demonstrated that zero backscattering can be realized at optical frequencies based on Kerker condition.[36] A silicon stair-like nanoantenna supported one electric dipole, two magnetic dipoles and one electric quadrupole is tailored to realize a radiation angle with a 20-degree range by tuning the geometric parameters of the nanoantenna.[37] Kerker condition can also be reached in high-index dielectric nanoparticles with electric, magnetic, and toroidal dipole moments.[38] Although it is shown that the backward scattering suppression can be achieved in a single high-index dielectric nanoparticle, the operating spectral regime in a non-resonant region and the scatterings in other directions is generally weak. To surmount the difficulty, a hybrid nanoantenna, i.e., a combination of metallic and dielectric nanoparticles, is introduced to realize a complementation of the directionality and radiation efficiency. A hybrid antenna with an electric dipole emitter longitudinally coupled to a silver dimer and transversely coupled to a GaP sphere is researched to control the direction of light scattering and characterize enhancement and radiation efficiency.[39,40] Hybrid metallo-dielectric core-shell spherical particles that offer tunable magnetic and electric resonances are widely investigated to establish Kerker scattering for backward scattering (BS) suppression and forward scattering (FS) enhancement.[41–44] The Kerker condition is also achieved by sub-wavelength plasmonic dimers formed by two silver strips separated by a thin dielectric spacer and embedded in a uniform dielectric medium.[45,46] The scattering of normally incident waves by core-shell nanowires, which support both electric and magnetic resonances is demonstrated that a pair of angles of vanishing scattering is obtained by generalizing the Kerker proposal for backward scattering suppression.[47] Most of the above researches realize Kerker condition in a single frequency, which limits more flexible applications to a certain extent.

In this paper, we show that hybrid metallo-dielectric core-shell nanorod, consisting of a gold core rod and a hollow silicon shell rod, can exhibit a dual-frequency Kerker condition for zero-backward scattering. Unlike the spherical core-shell structures,[42,43] this core-shell rod structure is more feasible in experiment fabrication on a substrate. In this structure, the metal core only supports strong electric resonance, the dielectric shell guarantees the existence of strong magnetic resonance and electric resonance, and the gap between core and shell plays an essential role in adjusting the overlaps of electric dipole and magnetic dipole resonances. The dual-frequency first Kerker scattering can be reached by manipulating the overlap of ED and MD moments in the spectrum. The hybrid nanorod model with an incident plane wave is simulated using finite element method (FEM) by COMSOL Multiphysics.[48] To comprehend accurately the physical connotation and action mechanism, the multipole expansion of the scattering field from hybrid nanorod is analyzed. We further explored directivity diagram's tendency when the distances between a point source incidence with hybrid nanorod change, which compared with the plane wave. The one-dimensional

(1D) arrays consist of hybrid nanorod (element number, N = 2, 4, 6) are also constructed to improve the directivity. The research investigated in this paper may extend the multi-functional applications of Kerker scattering and expand the scope of flexible construction methods to nanoantennas.

II. MULTIPOLE DECOMPOSITION

To analyze the electromagnetic properties of the hybrid nanorod theoretically and to demonstrate the first Kerker condition in the system, we employ multipole expansions when an incident plane wave interacts with a nanorod. We consider a plane wave with y polarized incident on a hybrid nanorod oriented transverse to the propagation direction ($+x$), as shown in Fig. 1. An approach to multipole decomposition of the optical theorem is the Taylor expansion of the exponential factor in the incident electric field. We can obtain multipole contributions of the field scattered from the nanorod using the definitions of the corresponding multipole moments,[49–52] which including the ED, MD, electric quadrupole moment (EQ), magnetic quadrupole moment (MQ), and toroidal dipole moment (TD).

The scattered far-field for homogeneous and substrate environments can be written as,[50–52]

$$\mathbf{E}_{SC}^{0,\,FF}(\mathbf{r}) \approx \omega^2 \mu_0 \frac{e^{ik_d(r - \mathbf{n}\cdot\mathbf{r}_0)}}{4\pi r}\left[\mathbf{n}\times(\mathbf{p}\times\mathbf{n}) - \frac{1}{v_d}(\mathbf{n}\times\mathbf{m})\right.$$
$$\left. + \frac{ik_d}{6}\left[\mathbf{n}\times(\mathbf{n}\times Q^e\mathbf{n})\right] + \frac{ik_d}{2v_d}(\mathbf{n}\times Q^m\mathbf{n})\right], \quad (1)$$

where ω is the angular frequency, $\mathbf{r}$ is the spatial coordinate vector, $\mu_0 = 4\pi\cdot10^{-7}$ H/m is the vacuum permeability, $v_d = c(\varepsilon_d)^{-1/2}$, c is the speed of light in vacuum, ε_d is the relative permittivity of dielectric surrounding, $r = |\mathbf{r}|$ and $\mathbf{n} = \mathbf{r}/r$ is the unit vector in the direction of observation, $\mathbf{p}(\mathbf{m})$ is the electric (magnetic) dipole moment, Q^e (Q^m) is the electric (magnetic) quadrupole tensor. The exact expressions of multipole moments can be written as follows and the TD can be seen as the higher order terms in the expansion of the electric dipole moments.[53–55]

$$\mathbf{p} = -\frac{1}{i\omega}\left\{\int d^3r J_\alpha^\omega j_0(kr) + \frac{k^2}{2}\int d^3r\left[3(r\cdot\mathbf{J}_\omega)r_\alpha - r2J_\alpha^\omega\right]\frac{j_2(kr)}{(kr)^2}\right\}$$
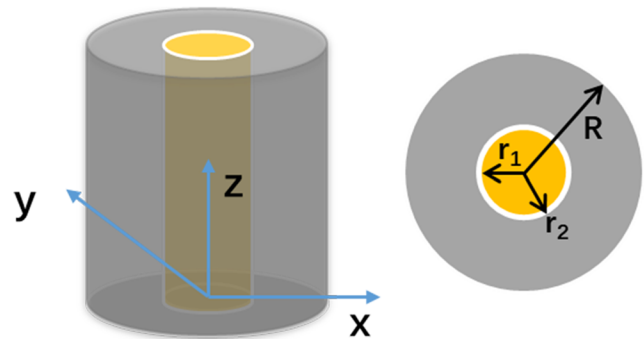$$(2)$$

FIG. 1. Schematic illustration of the metallo-dielectric hybrid nanorod.

$$\mathbf{m} = \frac{3}{2}\int d^3 r [\mathbf{r} \times \mathbf{J}_\omega]_\alpha \frac{j_1(kr)}{kr} \qquad (3)$$

$$\mathbf{Q}^e = -\frac{3}{i\omega}\left\{ \int d^3 r \left[3(r_\alpha J_\beta^\omega + J_\alpha^\omega r_\beta) - 2\delta_{\alpha\beta}(\mathbf{r}\cdot\mathbf{J}_\omega) \right]\frac{j_1(kr)}{kr} + 2k^2 \right.$$

$$\left. \times \int d^3 r \left[5 r_\alpha r_\beta(\mathbf{r}\cdot\mathbf{J}_\omega) - (r_\alpha J_\beta + J_\alpha r_\beta) - r^2\delta_{\alpha\beta}(\mathbf{r}\cdot\mathbf{J}_\omega) \right]\frac{j_3(kr)}{(kr)^3} \right\}$$

$$(4)$$

$$\mathbf{Q}^m = 15\int d^3 r \left\{ r_\alpha[\mathbf{r}\times\mathbf{J}_\omega]_\beta + r_\beta[\mathbf{r}\times\mathbf{J}_\omega]_\alpha \right\}\frac{j_2(kr)}{(kr)^2} \qquad (5)$$

$\mathbf{r}$ is distance vector from the origin to point (x, y, z) in the Cartesian coordinate system and the subscripts α, $\beta = x, y, z$ represent the components. The electric current density $\mathbf{J}_\omega$ is obtained by using $\mathbf{J}_\omega(r) = -i\omega\varepsilon_0(\varepsilon_r-\varepsilon_d)E_\omega(r)$, where $\varepsilon_0 = 8.845\cdot10^{-12}$ F/m is the permittivity of free space, ε_r is the relative permittivity of particle, $E_\omega(r)$ is electric field distribution. Multipole contributions show that the resonance peaks correspond to the overlap of several different multipole decomposition of the scattered field.

The time-averaged scattered powers of the multipoles can be written as the following summation,

$$I = \frac{1}{8\pi\varepsilon_0}\left[\frac{2\omega^4}{3c^3}|\mathbf{p}|^2 + \frac{2\omega^4}{3c^3}|\mathbf{m}|^2 + \frac{\omega^6}{20c^5}|\mathbf{Q}^e|^2 + \frac{\omega^6}{20c^5}|\mathbf{Q}^m|^2 \right]. \qquad (6)$$

And the scattering cross section C_{sca} can be defined,

$$C_{sca} = \frac{I}{I_{inc}}. \qquad (7)$$

Here, ω is the angular frequency, c is the speed of light in a vacuum, the higher order multipoles are not shown.

In order to investigate the conditions for zero-backward scattering, we consider an illustrative example in which a y-polarized plane wave propagates along the $+x$ direction and interacts with a nanorod in a homogeneous air environment, as shown in Fig. 1. The symmetry of this nanorod leads to an induced polarization current of the form $\mathbf{J}_p = (0, J_y, 0)^T$, which result in the only non-zero multipole components being p_y, m_z, T_y, $\mathbf{Q}^e_{xy} = \mathbf{Q}^e_{yx}$, $\mathbf{Q}^m_{yz} = \mathbf{Q}^m_{zy}$. The forward and backward scattered electric field along the x-direction which only contains the x-component is written as

$$\mathbf{E}_{SC,y}^{0,FF,+} = \omega^2\mu_0\frac{e^{ik_d(x+x_0)}}{4\pi r}\left[p_y + \frac{\sqrt{\varepsilon_r}}{c}m_z + \frac{k_d}{6}Q_{xy}^e + \frac{k_d}{2v_di}Q_{yz}^m \right], \quad (8)$$

$$\mathbf{E}_{SC,y}^{0,FF,-} = \omega^2\mu_0\frac{e^{ik_d(x+x_0)}}{4\pi r}\left[p_y - \frac{\sqrt{\varepsilon_r}}{c}m_z - \frac{k_d}{6}Q_{xy}^e + \frac{k_d}{2v_di}Q_{yz}^m \right]. \quad (9)$$

Therefore, to realize the zero-backward scattering (i.e., $\mathbf{E}_{SC,y}^{0,FF,-} = 0$), the equation below can be established,

$$p_y = \frac{\sqrt{\varepsilon_r}}{c}m_z, \qquad (10)$$

Eq. (10) is the well-known Kerker condition generalized to take into account dipole moments.

III. RESULTS AND DISCUSSIONS

The schematic descriptions of the metallo-dielectric core-shell hybrid nanorod structure are shown in Fig. 1. Here the core cylinder (Au) is embedded in shell hollow cylinder (Si) with a air gap between them, the sizes of hollow dielectric nanorod are defined by height H = 220 nm, external radius R = 120 nm and internal radius r_2 = 50 nm, and the radius of core metallic nanorod is r_1 = 48 nm. The refractive index of dielectric shell is n_1 = 3.5, and the dielectric functions of gold are taken from Palik's handbook.[56] To investigate the scattering properties of the hybrid nanorod in air surrounding medium (n_{air} =1), we consider a plane wave impinged to the hybrid nanorod along the x direction with a E_y polarization.

We start by investigating the scattering properties of individual silicon hollow nanorod with height H = 220 nm, external radius R = 120 nm, internal radius r_2 = 50 nm in a homogeneous air environment, as shown in Fig. 2. Owing to a high-index material and relatively low absorption losses in the visible and near-infrared, Si has been used in most previous work on magnetic resonances.[27,29,35,57–59] Based on Eq. (2) to Eq. (8), the multipole contributions are calculated respectively, which are distinguished by different colors and symbols in Fig. 2(a). The sum of them (gray triangle line) and the scattering cross-section (SCS, black solid line) are also simulated by FEM for comparison. The results in Fig. 2(a) show the normalized multipole contributions to SCS for the silicon hollow nanorod from 250 THz to 450 THz. The contributions of different modes in Fig. 2(a) are calculated by the different parts of Eq. (7). The sum of different contributions means the result of Eq. (7) in this way. And the SCS result is calculated by an integral of scattering power divided by incident power. All of the results are normalized by dividing a definite value (10^{-26} s·A^2/m) to more clearly show in figure. It is clear that the MD (red circle line) and ED (blue square line) resonance play the dominant roles of SCS, and the contributions of higher order multipole moments (i.e., EQ, MQ) are negligible relatively. The slight deviation between the sum of multipole contributions (gray triangle line) and the whole SCS (black solid line) may be caused by the coupling of mode and random error of FEM arithmetic. The forward scattering and backward scattering are determined as an integral of Poynting's vector in the semi-space with $x > 0$ and $x < 0$. The FS and BS strength are calculated respectively in the frequency range from 250 THz to 450 THz. The directionality is described as forward/backward scattering ratio, $G_{FB} = 20\log_{10}(|\mathbf{E}_{SC,y}^{0,FF,+}|/|\mathbf{E}_{SC,y}^{0,FF,-}|)$, where forward ($\mathbf{E}_{SC,y}^{0,FF,+}$) and backward ($\mathbf{E}_{SC,y}^{0,FF,-}$) scattered electric field along the x direction is defined in Eq. (8) and Eq. (9). Through calculating the G_{FB} spectra in Fig. 2(b), a sharp peak is observed at frequency 284 THz. Further calculated the 3D directional diagram in this frequency as shown as the inset of Fig. 2(b). It is obviously shown that the BS suppression and FS enhancement is realized.

To unambiguously clarify the contributions of different modes, the radiated far-field of nanoantenna with an induced electric dipole moment p_y (ED), magnetic dipole moment m_z (MD), which is characterized in Eq. (9) can be simplified as

$$\mathbf{E}_{SC,y}^{0,FF,-} = \omega^2\mu_0\frac{e^{ik_d(x+x_0)}}{4\pi r}\left[p_y - \frac{\sqrt{\varepsilon_r}}{c}m_z \right]. \qquad (11)$$
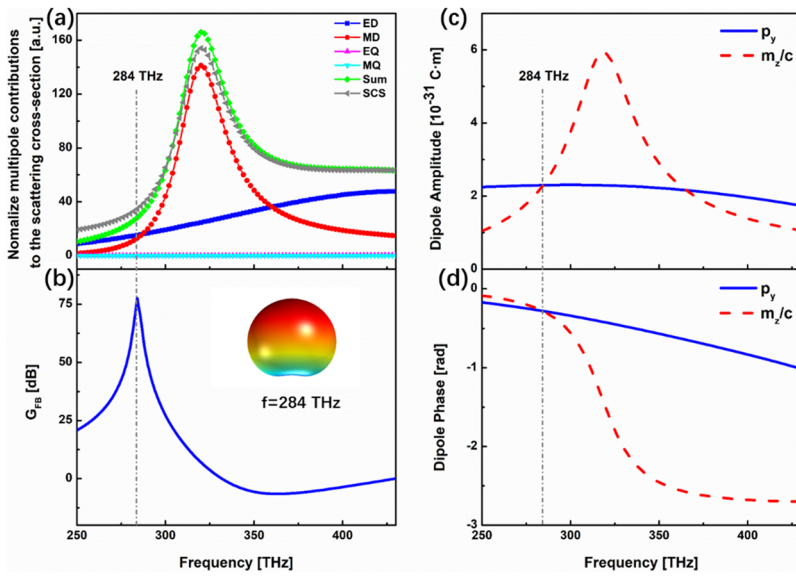
FIG. 2. (a) Frequency dependent normalized multipole contributions to the scattering cross-section for the silicon hollow nanorod with $H = 220$ nm, $R = 120$ nm, $r_2 = 50$ nm (b) Far-field forward to backward directionality (G_{FB}) spectra for the individual hollow silicon nanorod. Inset: the three-dimensional (3D) directional diagram of the nanoantenna at frequency 284 THz. The amplitude (c) and phase (d) of electric (p_y, blue solid line) and rescaled magnetic (m_z/c, red dash line) dipole moments of the individual silicon hollow nanorod.

Backward scattering can be exterminated if the first Kerker condition satisfied

$$p_y - \frac{\sqrt{\varepsilon_r}}{c} m_z = 0. \tag{12}$$

In this paper, we consider the air surrounding medium, the first Kerker condition can be represented as

$$p_y = m_z/c. \tag{13}$$

It can be seen that the amplitude and phase of p_y (blue solid line) are exactly equal to (m_y/c)'s at $f = 284$ THz in Fig. 2(c) and Fig. 2(d), where the Eq. (13) is satisfied. These results agree perfectly with the overlap of ED and MD contributions in Fig. 2(a) and the peak of G_{FB} in Fig. 2(b). Hence, the first Kerker condition explains the BS suppression and FS enhancement, as theoretically predicted. From 250 THz to 284 THz, p_y is approximately equal to m_z/c, which could generate unidirectionality too. As a result, G_{FB} is greater than zero from 250 THz to 284 THz, but less than the peak value where Kerker condition is satisfied. It is also noticed that the p_y and m_y/c have equal amplitude at the frequency of 366 THz, and the phase difference is 1.93 rad which is close to π. So, the ED and MD have equal amplitude, and are nearly in antiphase at 366 THz. This result is close to satisfying $\mathbf{E}_{SC,y}^{0,FF,+} = 0$, which results in the FS suppression and BS enhancement, as known as second Kerker condition. The valley in Fig. 2(b) means the FS suppression and BS enhancement near 366 THz, which is in accordance with the analysis of results in Fig. 2(c) and Fig. 2(d).

It is a truism that an isolated Au nanoantennas only supports electric dipolar resonance modes while higher ordered multipole ones remain dark.[60,61] When we combine the metal materials with the dielectric materials on nanoantennas, a strongly electric dipolar resonance is predicted to be introduced. As seen in the Fig. 3, the frequency dependent normalized multipole contributions to the SCS, G_{FB} spectra, p_y and m_z/c for the hybrid core-shell (Au-Si)

nanorod is calculated. By comparing the MD contribution (red circle line) of the single hollow dielectric nanorod (see Fig. 2(a)) and hybrid nanorod (see Fig. 3(a)), we can obviously observe that MD is almost unchanged. However, the ED contribution (blue square line) of the hybrid structure is larger than the one of the single hollow nanorod, due to the near-field coupling between EDs of the metallic and dielectric nanorods. For the hybrid nanoantenna, ED contribution to SCS is enhanced and changed forcefully while MD contribution remains unchanged, which lead to another overlap point occurs at higher frequency. The contributions of higher order multipole moments (i.e., EQ, MQ) are significantly smaller than the dipole moments, as shown in Fig. 3(a). It is reasonable to neglect the higher order multipole moments, because they have negligible effects on the SCS. There is an acceptable error between sums of multipole moments contributions (gray diamond line) and whole SCS (black solid line) simulated by FEM. There are two meaningful overlap points of ED and MD contributions at frequencies of 326 THz and 374 THz in Fig. 3(a), which is slightly deviated from G_{FB} peaks at frequencies of 324 THz and 380 THz in Fig. 3(b). The insets of Fig. 3(b) clearly show the 3D directional diagrams at 324 THz and 380 THz, which demonstrate the BS suppression and FS enhancement are reached in far-field.

From the Fig. 3(c) and Fig. 3(d), it is obviously shown that the amplitude and phase of p_y (blue solid line) are perfectly equal to amplitude and phase of m_z/c (red dash line) at frequency 324 THz respectively, and they are also close to overlapping at frequency 380 THz. In other words, the ED and MD have approximately equal amplitude and are nearly in phase at these two frequencies. The equivalences of p_y and m_z at 324 THz and 380 THz correspond with the G_{FB} spectra peaks, which illustrate the first Kerker condition is established to realize BS suppression and FS enhancement. Contrast to the former pure dielectric hollow nanorod supported electric and magnetic resonances, the introduce of metal nanorod supported electric resonance dramatically improved the ED, which result in the two overlap points with MD. Then the dual-frequency
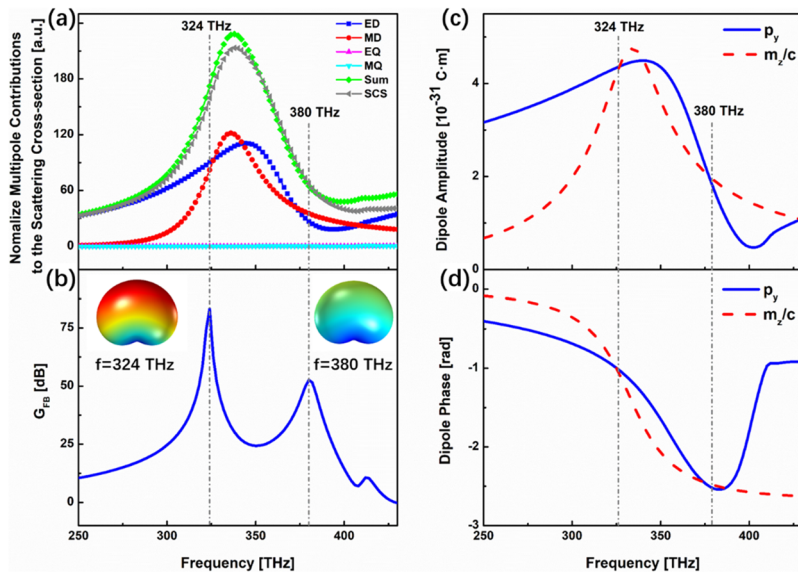
FIG. 3. (a) Frequency dependent normalized multipole contributions to the scattering cross-section for the core-shell (Au-Si) hybrid nanorod with H = 220 nm, R = 120 nm, r_2 = 50 nm, r_1 = 48 nm. (b) Far-field forward-to-backward directionality (G_{FB}) spectra for the hybrid nanorod. Inset: the 3D directional diagram of the nanoantenna at frequency 324 THz and 380 THz. The amplitude (c) and phase (d) of electric (p_y, blue solid line) and rescaled magnetic (m_z/c, red dash line) dipole moments of the hybrid nanorod.

first Kerker conditions are realized. When the amplitude and phase slightly deviate from the Kerker condition, the radiation pattern can still exhibit. As shown in Fig. 3(c) and Fig. 3(d), the ED and MD have approximate amplitude and phase in a broad band from 250 THz to 400 THz. Therefore, G_{FB} spectra results in Fig. 3(b) show that the hybrid nanoantenna exhibit remarkable directionality in a broad band of 150 THz. From the foregoing, the dual-frequency

first Kerker conditions provide an extra degree of freedom for light scattering control through interfering electric and magnetic multipoles, and may widen the versatile applications in nanoantennas, biosensing, light emission and photovoltaic devices.

To better verify the results of the far-field calculation and demonstrate the mechanism of directional emission, the 2D directional diagrams in E-plane (xy plane) and H-plane (xz plane) is
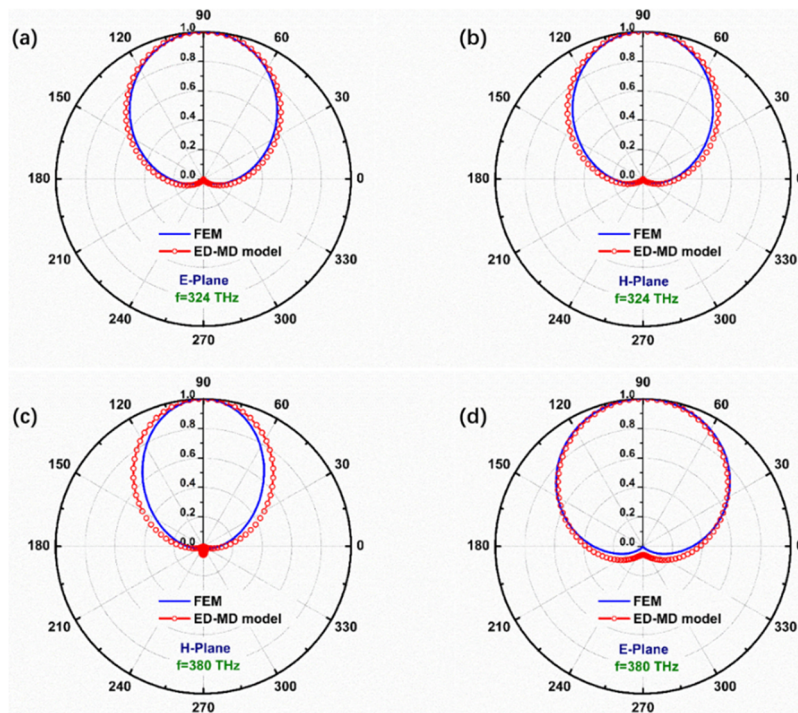

FIG. 4. Two-dimensional (2D) directional diagrams in E-plane (xy plane) and H-plane (xz plane) calculated by the FEM (blue solid curves) and the analytical ED-MD model (red circle curves) at 324 THz and 380 THz resonances for hybrid nanorod. (a) E-plane at 324 THz. (b) H-plane at 324 THz. (c) E-plane at 380 THz. (d) H-plane at 380 THz.

respectively calculated by the FEM (blue solid curves) and the analytical ED-MD model (red circle curves) at 324 THz and 380 THz resonances for hybrid nanorod, as shown in Fig. 4. The results of FEM are analyzed by full-wave electromagnetic calculations, and the results of ED-MD interference model are calculated by Eq. (1) taken into account the dominant multipole moments (ED and MD). The induced p_y and m_z are calculated numerically as p_y = (-2.31+3.59i)×10^{-31} C·m, m_z/c = (-2.41+3.20i)×10^{-31} C·m for 324 THz, and p_y = (1.33+1.23i)×10^{-31} C·m, m_z/c = (1.63 +1.23i)×10^{-31} C·m for 380 THz, which are calculated by Eq. (2) and Eq. (3) in Fig. 4. The results of FEM and ED-MD model are almost coincident. The slight deviations may be attributed to negligible contributions from the higher-order multipoles or the couplings of multipole modes, which are not accounted for in the D-M model. It is demonstrated that the scattering cross section depend on ED and MD, and the calculation results from FEM are credible compared with theoretical analysis.

In order to explore the properties of hybrid nanoantenna under electric dipole excitation, an electric dipole emitter is located on a point with a distance d from nanoantenna along the x-direction, as shown in Fig. 5(a). The results of G_{FB} spectra with different distance d (10, 20, 30, 40, 50 nm) are shown in Fig. 5(b). There are two peaks of G_{FB} spectra at 350 THz to 408 THz, which are analogous to the FS/BS scattering spectra in Fig. 3(b) calculated with plane wave incidence. The differences between them are the frequency shifts about 7%, as a result of the phase retardation effect.[34,62] It's worth noting that with the increasing of d, the peaks have the tendency of the slight shift to low frequency. The reason of this tendency can be interpreted as that the near-field coupling weakens with the distance d increasing.[63] The electromagnetic wave excited by electric dipole can be treated as plane waves while the distance d is large enough. The normalized 2D far-field scattering patterns of E-plane corresponding to the frequency of 350 THz and 408 THz with different d are shown in Figs. 5(c) and 5(d). With the increase of d,

the BS separations are strengthening while the FS enhancements are weak relatively at both two frequencies. Note that the BS suppressions are weaken with the decrease of distance d, owing to the interference and coupling of original single emitter, induced electric dipole and induced magnetic dipole.[64] Based on these results, the scattering properties are demonstrated that the dual-frequency Kerker condition can be realized both with electric dipole emitter and with plane wave, and the results agree well with theoretical analysis.

The practical application value is an evergreen discussion of a theoretical model. For the guiding significance of experimental preparation and practical application, an emitter-antenna system is designed and simulated, as shown in Fig. 6. Considering experimental fabrication and measurement, the emitter-antenna system consists of electric dipole source with y-direction polarization and hybrid nanoantenna which is placed on a glass substrate (ε_d = 2.25). The normalized 2D radiation patterns in xz plane at the peak frequencies (324 THz and 380 THz) shown in Fig. 5(b) are simulated and graphed in Figs. 6(b) and 6(c). The maximum scattering is directed toward the composition of substrate direction and $+x$ direction, due to most of the light is scattered into the higher index substrate, the ideal scattering pattern in free space is disturbed.[65] The possible reason is analyzed, the dielectric constant of substrate (ε_d = 2.25) is close to silica nanorod (n_1 = 3.5). Compared to air, the impedance matching between substrate and dielectric nanorod is easier to achieve, which leads to the energy tend to enter substrate more than air. Therefore, based on these results, the hybrid nanoantenna could be fabricated and measured experimentally to realize dual-frequency first Kerker condition.

Up to now, we have demonstrated azimuthally symmetric unidirectional scattering using a single core-shell nanorod. To further enhance the directionality, we employ a 1D chain of such hybrid nanorods with a chain axis parallel to the polarized direction of the incident plane wave, where the interrod distance is D = 180 nm
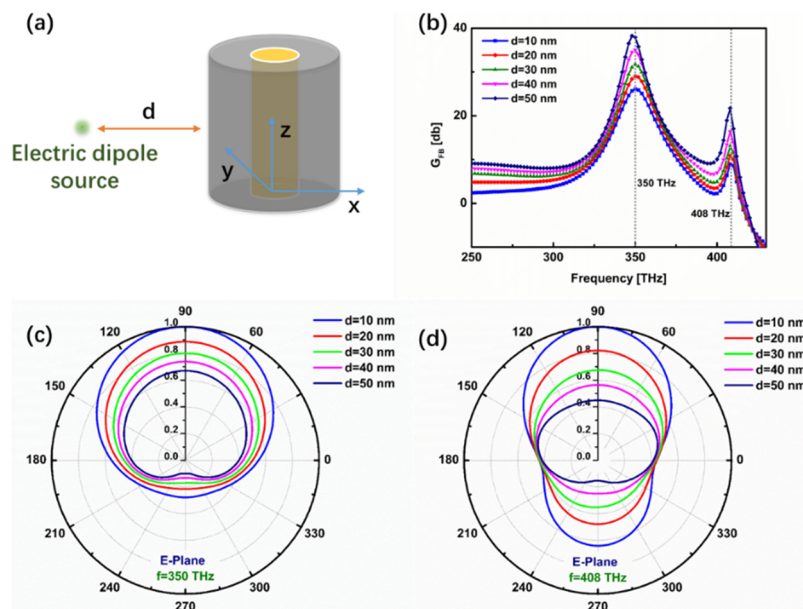

FIG. 5. Electric dipole source excitation. (a) Schematic of the hybrid nanoantenna excited by an y-polarized electric dipole emitter. (b) Far-field forward-to-backward directionality G_{FB} versus frequency with different d. (c) 2D directional diagrams corresponding to the frequency of 350 THz with different d. (d) 2D directional diagrams corresponding to the frequency of 408 THz with different d.
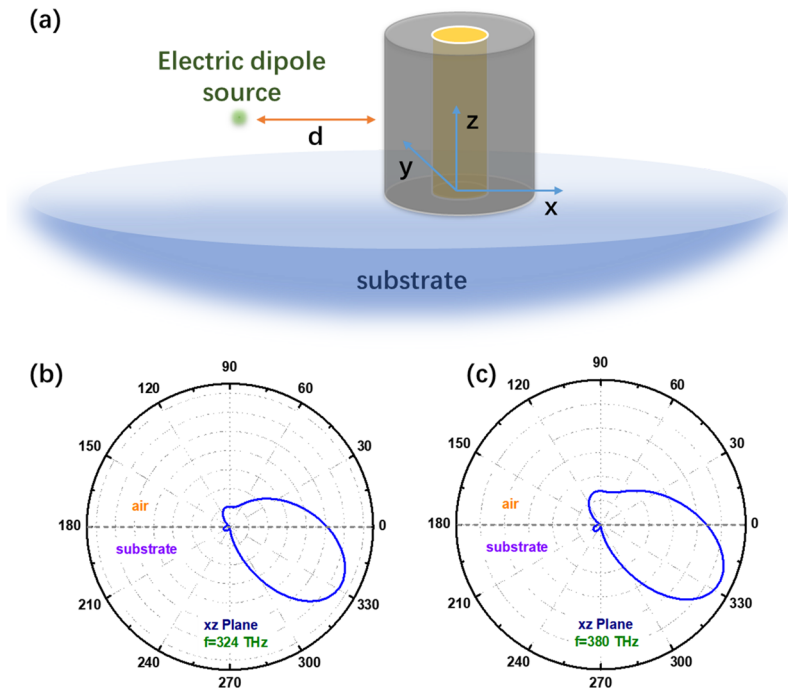
FIG. 6. (a) The schematic of emitter-antenna system placed on a glass substrate (ε_d = 2.25). (b) and (c) Normalized 2D radiation patterns in *xz* plane at the resonance frequencies, 324 THz and 380 THz, respectively. The substrate fills the half-space from 180° to 360°.
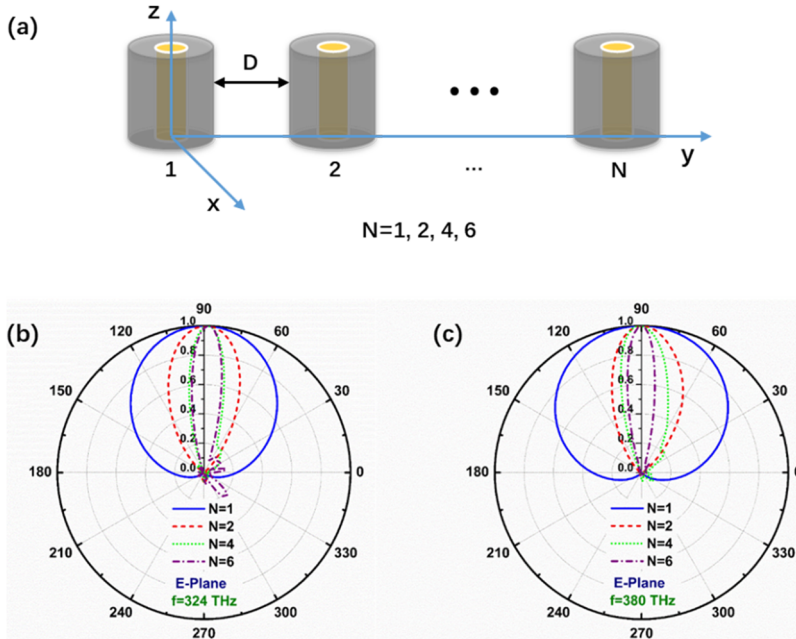

FIG. 7. (a) The schematic of 1D arrays of dielectric nanorods with spacing *D* along the *y* direction. (b) and (c) Normalized 2D far field directional diagrams in the E-plane by 1D arrays of hybrid nanorods with N = 1, 2, 4, and 6 nanorods at 324 THz and 380 THz resonance, respectively.

(see Fig. 7(a)). The designed 1D array structures of the hybrid nanorods are expected to optimize the scattering properties of nanoantenna. Figure. 7(b) and 7(c) has shown the normalized 2D far-field directional diagrams of E-plane with different *N* (*N* =1, 2, 4, and 6) at 324 THz and 380 THz which corresponding to the peak frequencies of FB to BW spectra for the single rod. It is clear from Figs. 7(b) and 7(c) that, by increasing the number of rods, the main

lobe beamwidth will decrease, indicating a better directionality and this due to the constructive far-field interferences.[34,42]

IV. CONCLUSION

In summary, the dual-frequency zero-backward scattering is reached in a hybrid metallo-dielectric core-shell nanorod with the

first Kerker condition gained. To reveal the action mechanism and intrinsic rules, the frequency dependent normalized multipole contributions to the SCS for the hollow dielectric (Si) nanorod and hybrid core-shell (Au-Si) nanorod are both calculated. In contrast to the dielectric nanorod, the ED moments of hybrid nanorod are enhanced and adjusted to overlap with MD contributions, which generate the first Kerker conditions at 324 THz and 380 THz. An analytical dipole model is established, which yields comparable results to those from the full wave simulation. Furthermore, an electric dipole source with a distance d from nanoantenna is applied and realized dual-frequency first Kerker condition in analogy with the results of plane wave incidence. The dual-frequency zero-backward scattering can be further optimized by 1D nanoantenna array, it is demonstrated that the direction angles are decreased with the unit number increasing. The proposed dual-frequency zero-backward scattering with highly unidirectionality and controllability may lead to further extend and applied in sensing, nanoantenna and nanophotonic.

ACKNOWLEDGMENTS

REFERENCES

[1] E. Huber and M. Frost, *Light scattering by small particles* (Wiley, 1957).

[2] M. Kerker, *The scattering of light, and other electromagnetic radiation* (Academic Press, London, UK, 1969).

[3] R. Huschka, J. Zuloaga, M. W. Knight, L. V. Brown, P. Nordlander, and N. J. Halas, "Light-induced release of DNA from gold nanoparticles: Nanoshells and nanorods," J. Am. Chem. Soc. **133**, 12247–12255 (2011).

[4] D. Sikdar, W. Cheng, and M. Premaratne, "Optically resonant magneto-electric cubic nanoantennas for ultra-directional light scattering," J. Appl. Phys. **117**(8), 083101 (2015).

[5] H. Alisafaee and M. A. Fiddy, "Nanoantennas for nanodisk photovoltaics," Appl. Phys. Lett. **105**(11), 113107 (2014).

[6] W. Wan, W. Zheng, Y. Chen, and Z. Liu, "From Fano-like interference to superscattering with a single metallic nanodisk," Nanoscale **6**(15), 9093–9102 (2014).

[7] M. E. Stewart, C. R. Anderton, L. B. Thompson, J. Maria, S. K. Gray, J. A. Rogers, and R. G. Nuzzo, "Nanostructured plasmonic sensors," Chem. Rev. **108**(2), 494–521 (2008).

[8] R. Alaee, R. Filter, D. Lehr, F. Lederer, and C. Rockstuhl, "A generalized Kerker condition for highly directive nanoantennas," Opt. Lett. **40**(11), 2645–2648 (2015).

[9] R. Alaee, C. Menzel, U. Huebner, E. Pshenay-Severin, S. B. Hasan, T. Pertsch, C. Rockstuhl, and F. Lederer, "Deep-subwavelength plasmonic nanoresonators exploiting extreme coupling," Nano Lett. **13**(8), 3482–3486 (2013).

[10] L. Verslegers, Z. Yu, Z. Ruan, P. B. Catrysse, and S. Fan, "From electromagnetically induced transparency to superscattering with a single structure: A coupled-mode theory for doubly resonant structures," Phys. Rev. Lett. **108**(8), 083902 (2012).

[11] Y. J. Feng, S. Xiong, X. F. Xu, B. Zhu, J. M. Zhao, and T. Jiang, "Dielectric multi-layers for antenna and cloaking devices designed from transformation electromagnetics," in Ursi International Symposium on Electromagnetic Theory, 872–875 (2013).

[12] A. E. Krasnok, A. E. Miroshnichenko, P. A. Belov, and Y. S. Kivshar, "All-dielectric optical nanoantennas," Opt. Express **20**(18), 20599–20604 (2014).

[13] S. Person, M. Jain, Z. Lapin, J. J. Saenz, G. Wicks, and L. Novotny, "Demonstration of zero optical backscattering from single nanoparticles," Nano Lett. **13**(4), 1806–1809 (2013).

[14] L. Novotny and N. V. Hulst, "Antennas for light," Nat. Photonics **5**, 83 (2011).

[15] N. S. King, M. W. Knight, A. M. Goodman, P. Nordlander, and N. J. Halas, "Orienting nanoantennas in three dimensions to control light scattering across a dielectric interface," Nano Lett. **13**, 5997–6001 (2013).

[16] B. García-Cámara, F. Moreno, F. González, and O. J. Martin, "Light scattering by an array of electric and magnetic nanoparticles," Opt. Express **18**, 10001 (2010).

[17] A. V. Kabashin, P. Evans, S. Pastkovsky, W. Hendren, G. A. Wurtz, R. Atkinson, R. Pollard, V. A. Podolskiy, and A. V. Zayats, "Plasmonic nanorod metamaterials for biosensing," Nat. Mat. **8**, 867–871 (2009).

[18] S. R. Rodriguez, A. F. Bernal, T. P. Steinbusch, M. A. Verschuuren, A. F. Koenderink, and R. J. Gómez, "Breaking the symmetry of forward-backward light emission with localized and collective magnetoelectric resonances in arrays of pyramid-shaped aluminum nanoparticles," Phys. Rev. Lett. **113**, 247401 (2014).

[19] H. A. Atwater and A. Polman, "Plasmonics for improved photovoltaic devices," Nature Materials **9**, 205–213 (2010).

[20] M. Kerker, D.-S. Wang, and C. L. Giles, "Electromagnetic scattering by magnetic spheres," J. Opt. Soc. Am. **73**, 765–767 (1983).

[21] A. Pors, S. K. Andersen, and S. I. Bozhevolnyi, "Unidirectional scattering by nanoparticles near substrates: Generalized Kerker conditions," Opt. Express **23**, 28808–28828 (2015).

[22] I. M. Hancu, A. G. Curto, M. Castro-Lopez, M. Kuttge, and N. F. van Hulst, "Multipolar interference for directed light emission," Nano Lett. **14**, 166–171 (2014).

[23] S. M. Hein and H. Giessen, "Tailoring magnetic dipole emission with plasmonic split-ring resonators," Phys. Rev. Lett. **111**, 026803 (2013).

[24] S. Varault, B. Rolly, G. Boudarham, G. Demesy, B. Stout, and N. Bonod, "Multipolar effects on the dipolar polarizability of magneto-electric antennas," Opt. Express **21**, 16444–16454 (2013).

[25] K. Yao and Y. M. Liu, "Controlling electric and magnetic resonances for ultra-compact nanoantennas with tunable directionality," ACS Photonics **3**, 953–963 (2016).

[26] S. N. Sheikholeslami, A. Garcia-Etxarri, and J. A. Dionne, "Controlling the interplay between electric and magnetic modes via Fano-like plasmon resonances," Nano Lett. **11**, 3927–3934 (2011).

[27] A. I. Kuznetsov, A. E. Miroshnichenko, Y. H. Fu, J. Zhang, and B. Luk'yanchuk, "Magnetic light," Sci. Rep. **2**, 492 (2012).

[28] L. Shi, J. T. Harris, R. Fenollosa, I. Rodriguez, X. Lu, B. A. Korgel, and F. Meseguer, "Monodisperse silicon nanocavities and photonic crystals with magnetic response in the optical region," Nat. Commun. **4**, 1904 (2013).

[29] A. García-Etxarri, R. Gómez-Medina, L. S. Froufe-Pérez, C. López, L. Chantada, F. Scheffold, J. Aizpurua, M. Nieto-Vesperinas, and J. J. Sáenz, "Strong magnetic response of submicron silicon particles in the infrared," Opt. Express **19**, 4815–4826 (2011).

[30] M. K. Schmidt, R. Esteban, J. J. Sáenz, I. Suárez-Lacalle, S. Mackowski, and J. Aizpurua, "Dielectric antennas–A suitable platform for controlling magnetic dipolar emission," Opt. Express **20**, 13636–13650 (2012).

[31] F. Neubrech, A. Pucci, T. W. Cornelius, S. Karim, A. García-Etxarri, and J. Aizpurua, "Resonant plasmonic and vibrational coupling in a tailored nanoantenna for infrared detection," Phys. Rev. Lett. **101**, 157403 (2008).

[32] T. Shibanuma, P. Albella, and S. A. Maier, "Unidirectional light scattering with high efficiency at optical frequencies based on low-loss dielectric nanoantennas," Nanoscale **8**, 14184–14192 (2016).

[33] J. van de Groep and A. Polman, "Designing dielectric resonators on substrates: Combining magnetic and electric resonances," Opt. Express **21**, 26285–26302 (2013).

[34] X. M. Zhang, Q. Zhang, S. J. Zeng, Z. Z. Liu, and J. J. Xiao, "Dual-band unidirectional forward scattering with all-dielectric hollow nanodisk in the visible," Opt. Lett. **43**, 1275–1278 (2018).

[35] Y. H. Fu, A. I. Kuznetsov, A. E. Miroshnichenko, Y. F. Yu, and B. Luk'yanchuk, "Directional visible light scattering by silicon nanoparticles," Nat. Commun. **4**, 1527 (2013).

[36]S. Person, M. Jain, Z. Lapin, J. J. Saenz, G. Wicks, and L. Novotny, "Demonstration of zero optical backscattering from single nanoparticles," Nano Lett. **13**, 1806–1809 (2013).

[37]J. Tian, Q. Li, Y. Yang, and M. Qiu, "Tailoring unidirectional angular radiation through multipolar interference in a single-element subwavelength all-dielectric stair-like nanoantenna," Nanoscale **8**, 4047–4053 (2016).

[38]P. D. Terekhov, K. V. Baryshnikova, A. S. Shalin, A. Karabchevsky, and A. B. Evlyukhin, "Resonant forward scattering of light by high-refractive-index dielectric nanoparticles with toroidal dipole contribution," Opt. Lett. **42**, 835–838 (2017).

[39]B. Rolly, B. Stout, and N. Bonod, "Boosting the directivity of optical antennas with magnetic and electric dipolar resonant particles," Opt. Express **20**, 20376–20386 (2012).

[40]X. Zeng, W. Yu, P. Yao, Z. Xi, Y. Lu, and P. Wang, "Metallo-dielectric hybrid antenna for high Purcell factor and radiation efficiency," Opt. Express **22**, 14517–14523 (2014).

[41]R. Paniagua-Domínguez, F. López -Tejeira, R. Marqués, and J. A. Sánchez-Gil, "Metallo-dielectric core–shell nanospheres as building blocks for optical three-dimensional isotropic negative-index metamaterials," New J. Phys. **13**, 123017 (2011).

[42]W. Liu, A. E. Miroshnichenko, D. N. Neshev, and Y. S. Kivshar, "Broadband unidirectional scattering by magneto-electric core–shell nanoparticles," ACS Nano **6**, 5489–5497 (2012).

[43]Y. Li, M. Wan, W. Wu, Z. Chen, P. Zhan, and Z. Wang, "Broadband zero-backward and near-zero-forward scattering by metallo-dielectric core-shell nanoparticles," Sci. Rep. **5**, 12491 (2015).

[44]G. Pellegrini, P. Mazzoldi, and G. Mattei, "Asymmetric plasmonic nanoshells as subwavelength directional nanoantennas and color nanorouters: A multipole interference approach," J. Phys. Chem. C **116**, 21536–21546 (2012).

[45]E. Poutrina, A. Rose, D. Brown, A. Urbas, and D. R. Smith, "Forward and backward unidirectional scattering from plasmonic coupled wires," Opt. Express **21**, 31138–31154 (2013).

[46]E. Poutrina and A. Urbas, "Multipole analysis of unidirectional light scattering from plasmonic dimers," J. of Opt. **16**, 114005 (2014).

[47]W. Liu, A. E. Miroshnichenko, R. F. Oulton, D. N. Neshev, O. Hess, and Y. S. Kivshar, "Scattering of core-shell nanowires with the interference of electric and magnetic resonances," Opt. Lett. **38**, 2621–2624 (2013).

[48]http://www.comsol.com.

[49]J. D. Jackson, *Classical Electrodynamics*, 3rd ed. (Wiley, 1999).

[50]A. B. Evlyukhin, T. Fischer, C. Reinhardt, and B. N. Chichkov, "Optical theorem and multipole scattering of light by arbitrarily shaped nanoparticles," Phys. Rev. B **94**, 205434 (2016).

[51]A. B. Evlyukhin, C. Reinhardt, A. Seidel, B. S. Luk'Yanchuk, and B. N. Chichkov, "Optical response features of Si-nanoparticle arrays," Phys. Rev. B **82**, 045404 (2010).

[52]A. E. Miroshnichenko, A. B. Evlyukhin, Y. F. Yu, R. M. Bakker, A. Chipouline, A. I. Kuznetsov, B. Luk'Yanchuk, B. N. Chichkov, and Y. S. Kivshar, "Nonradiating anapole modes in dielectric nanoparticles," Nat. Commun. **6**, 8069 (2015).

[53]R. Alaee, C. Rockstuhl, and I. Fernandez-Corbaton, "An electromagnetic multipole expansion beyond the long-wavelength approximation," Opt. Commun. **407**, 17–21 (2018).

[54]E. E. Radescu and G. Vaman, "Exact calculation of the angular momentum loss, recoil force, and radiation intensity for an arbitrary source in terms of electric, magnetic, and toroid multipoles," Phys. Rev. E **65**, 046609 (2002).

[55]X. Zhang, S. Wang, Z. Lin, H. B. Sun, and C. T. Chan, "Optical force on toroidal nanostructures: Toroidal dipole versus renormalized electric dipole," Phys. Rev. A **92**(4), 043804 (2015).

[56]E. D. Palik, *Handbook of Optical constants of Solids* (Academic Press, New York, 1985).

[57]A. B. Evlyukhin, S. M. Novikov, U. Zywietz, R. L. Eriksen, C. Reinhardt, S. I. Bozhevolnyi, and B. N. Chichkov, "Demonstration of magnetic dipole resonances of dielectric nanospheres in the visible region," Nano Lett. **12**, 3749–3755 (2012).

[58]P. Spinelli, M. A. Verschuuren, and A. Polman, "Broadband omnidirectional antireflection coating based on subwavelength surface Mie resonators," Nat. Commun. **3**, 692 (2012).

[59]I. Staude, A. E. Miroshnichenko, M. Decker, N. T. Fofang, S. Liu, E. Gonzales, J. Dominguez, T. S. Luk, D. N. Neshev, I. Brener, and Y. Kivshar, "Tailoring directional scattering through magnetic and electric resonances in subwavelength silicon nanodisks," ACS Nano **7**(9), 7824–7832 (2013).

[60]F. Hao, E. Larsson, T. Ali, D. Sutherland, and P. Nordlander, "Shedding light on dark plasmons in gold nanorings," Chem. Phys. Lett. **458**(4-6), 262–266 (2008).

[61]J. Aizpurua, P. Hanarp, D. S. Sutherland, M. Käll, G. W. Bryant, and F. J. García de Abajo, "Optical properties of gold nanorings," Phys. Rev. Lett. **90**(5), 057401 (2003).

[62]X. M. Zhang, J. J. Xiao, Q. Zhang, F. Qin, X. Cai, and F. Ye, "Dual-band unidirectional emission in a multilayered metal–dielectric nanoantenna," ACS Omega **2**, 774–783 (2017).

[63]Q. Zhang, J. J. Xiao, X. M. Zhang, Y. Yao, and H. Liu, "Reversal of optical binding force by Fano resonance in plasmonic nanorod heterodimer," Opt. Express **21**, 6601–6608 (2013).

[64]Y. Yang, Q. Li, and M. Qiu, "Controlling the angular radiation of single emitters using dielectric patch nanoantennas," Appl. Phys. Lett. **107**, 031109 (2015).

[65]D. Vercruysse, Y. Sonnefraud, N. Verellen, F. B. Fuchs, G. D. Martino, L. Lagae, V. V. Moshchalkov, S. A. Maier, and P. V. J. N. L. Dorpe, "Unidirectional side scattering of light by a single-element nanoantenna," Nano Lett. **13**(8), 3843 (2013).